Rupture Passing Probabilities at Fault Bends and Steps, With Application to Rupture Length Probabilities For Earthquake Early Warning

Glenn P. Biasi[1]
gbiasi@usgs.gov
Steven G. Wesnousky[2]
wesnousky@unr.edu

[1] U.S. Geological Survey, 525 S. Wilson Avenue, Pasadena, CA 91106
[2] Center for Neotectonic Studies and Seismological Laboratory, University of Nevada, Reno, NV 89557, USA.

Keywords. Earthquake Hazards, California,

Abstract

Earthquake early warning (EEW) systems can quickly identify the onset of an earthquake rupture, but the first few seconds of seismic data only weakly predict the final rupture length. We present two approaches for estimating the conditional probabilities of rupture length given a nucleation point from an EEW system. Bends and steps in a fault are geometric complexities with some probability of arresting rupture. Their effects compound serially with rupture length, and provide a physical basis for probabilistic estimates of where rupture may stop. Applied to a discretized fault model for California, geologically reasonable probabilities of length are found. For an example rupture initiated on the central San Jacinto fault (SJF) 70 km SE of the intersection with the San Andreas fault (SAF), 78% grow to **M** 6.3, 8% become **M** ~7.1 and reach the connection to the SAF, and less than 1% reach 300 km and **M** 7.7 or larger. For the same nucleation point on the SJF, conditional probabilities of length calculated from Uniform California Earthquake Rupture Forecast v3 (UCERF3) rupture rates predict 18% would reach the San Andreas fault, and about 13% will reach 300 km or larger. From geometric complexity, most ruptures on the SAF starting at Bombay Beach in the southern Salton Trough are arrested in the complex Mill Creek section, and only ~5% reach to San Bernardino and become an acute hazard to Los Angeles. Conditional probabilities of length can be precompiled and are of potential use to EEW both for alert planning and operations.

Introduction

Earthquake early warning (EEW) systems are designed to warn of pending strong shaking from a large earthquake by exploiting the speed advantage of electronically transmitted signals over seismic waves (Cooper, 1868; Heaton, 1985; Kanamori et al., 1997). Efforts to develop, formalize, and apply, EEW methodologies in California have moved forward in concert with advances in seismic instrumentation, telemetry, computers, data storage, and real-time seismological analysis (Chung et al., 2019; Cochran et al., 2019, Kohler et al., 2018; Allen and Kanamori, 2003; Allen et al., 2009; Heaton, 1985; Kanamori et al., 1997; Kanamori et al., 1999; Kanamori, 2005; Wu and Teng, 2002). Methodologies generally entail the rapid estimation of the magnitude of an earthquake from observations of peak displacement, velocity, and acceleration (Wu and Kanamori, 2005; Wu et al., 2007; Wu and Kanamori, 2008) or the predominant period and frequency content (Allen and Kanamori, 2003; Kanamori, 2005; Nakamura, 1988) of the first seconds of the first recorded P-wave.

The actual moment released in the first seconds of a large earthquake normally corresponds to an M 6 to 6.5 earthquake. Early work suggested that the eventual magnitude of an earthquake that continues to grow could be known from how it starts (Olson and Allen, 2005). Later studies have questioned this conclusion, and find instead that reliable estimates of final magnitude require more data, from extended P-wave displacements (Yamada and Ide, 2008; Noda and Ellsworth, 2016), up to half or more of the rupture itself (Meier et al., 2016; Trugman et al., 2019). To estimate magnitude and rupture extent of larger earthquakes, the ShakeAlert system includes an algorithm named FinDER (Bose et al., 2012). FinDER estimates event size based on a finite fault model of rupture and ground motion template matching to observed ground motions. The alternative Propagation of Undamped Motion algorithm (PLUM, Kodera, 2018) avoids magnitude estimation altogether and instead predicts alert areas from locations of observed strong ground motions and a forward model of ground motion for growth of the alert area. Originally developed in Japan, PLUM is under evaluation for the ShakeAlert system (Cochran et al., 2019).

In this paper we present a probabilistic approach for estimating the eventual length of a growing earthquake rupture given the starting location and knowledge of the fault structure. Probabilities conditioned on alert location can be computed in advance for all discrete elements in the fault system. We also develop an alternative approach to integrate the Uniform California Earthquake Rupture Forecast

version 3 (UCERF3; Field et al., 2014; Field et al., 2017) into EEW. A priori estimates of rupture length cannot take the place of direct measurement of the rupture under way, but may be useful, for example, to inform policies for alert area as a function of initial earthquake magnitude and location.

Estimating Probable Length of Future Earthquakes

Discretized Fault Model

On a long-term basis, a fault-based rupture forecast such as UCERF3 in California can be used to estimate of the likelihood that a rupture of a given length will occur. However, once a rupture has started, the a priori probabilities of earthquake occurrence no longer apply, and the length estimate becomes conditional on the starting location and the fault structure connected to it.

To introduce our approach to estimating the probability of eventual rupture length conditioned on knowledge of initial location, we begin with a simplified discrete fault model (**Figure** 1). Each subsection models an area nominally ruptured by the time an EEW point source algorithm could alert and identify that a rupture is under way and could grow. The fault consists of 9 subsections, and we assume that rupture initiates in the middle, as rupture of panel S_0. Given rupture initiation in S_0 and the 9-element discrete model shown, there are 24 possible rupture extensions (**Figure 1)**. If all rupture extents are equally likely (i.e. $p_1=p_2=p_3$ etc.), then by total probability one may simply count the ruptures with the extent of interest as a fraction of all possibilities. For example, ruptures *1-4* have unilateral rupture to the right (*ur*) of panel S_0, so $P_{ur} = \sum_{i=1}^{4} p_i$ Unilateral rupture to the left (*ul*) of panel S_0 is $P_{ul} = \sum_{i=5}^{8} p_i$, and the probability of a bilateral rupture (*bl*) is $P_{bl} = \sum_{i=9}^{24} p_i$. Other cases such as starting in S_0 and ending in panel S_3 (either bilateral or unilateral) follow by summing the probabilities of the individual ruptures. Thus, in this simplest model where all ruptures are equally likely, given a rupture initiates in S_0, one may simply count the ruptures involving each of the other subsections (**Figure 2a)** and translate to probabilities by dividing by the total number of ruptures (bar heights, **Figure 2b)**.

Modifying the Discretized Model - Magnitude-Frequency Distribution

A problem with the simple fault model of **Figure 1** is that, observationally, larger magnitude and thus longer ruptures occur less frequently than shorter ones. One path forward for adjusting rupture length expectations is to apply a fault magnitude-frequency distribution (MFD). The exact form of the MFD appropriate to describe the recurrence of large (>M6 – 6.5) earthquakes on long faults remains a topic of discussion, but the power-law Gutenberg-Richter (GR) MFD provides a relevant reference. In a GR distribution, the number of earthquakes equal or exceeding some magnitude **M** is given by $logN(\boldsymbol{M}) = a - b*\boldsymbol{M}$. Typically, and in California, the value of *b* is found to be near 1. We convert model lengths to magnitudes using **M-***L* relationships of Anderson et al. (2017). The value of *a* is not required because of the condition that the event has initiated, and only the relative frequency of larger events is thus of interest. The effect of assuming the power law frequency distribution is to progressively decrease probabilities with increasing rupture length (**Figure 2b)**.

Table 1 lists the predicted relative frequencies of events by magnitude. To tabulate length or magnitude), N(**M**) includes all events of a given length. For example, three ruptures including S_0 have length 21 km (S_2-S_1-S_0, S_1-S_0-S_{-1}, and S_0-S_{-1}-S_{-2}). The frequency of any one of the three (absent other information) is thus from **Table 1** N(**M**)=0.110/3. **Table 1** immediately provides a useful reference. For example, only 25% ruptures are predicted to grow to occupy a second subsection, and only 2% would go on to become an **M** 7.0 event.

Table 1. Final rupture length and frequency of length given a 7-km initial rupture.

Length (km)	7	14	21	28	35	42	49	56	63
Mw	5.33	5.94	6.29	6.54	6.73	6.89	7.02	7.14	7.24
N(M) ratio	1.000	0.246	0.110	0.062	0.040	0.028	0.020	0.016	0.012

Modifying the Discretized Model - Fault Geometry

Faults and Bends

In the simple fault model of **Figure 1** rupture can proceed from one panel to the next without penalty. Empirical observations and computer models of rupture processes indicate that geometrical complexities such as steps and bends affect the probability that rupture will stop (e.g., Biasi and Wesnousky, 2016; Biasi and Wesnousky, 2017; Lettis et al., 2002; Harris et al., 1991; Lozos et al., 2011; Lozos et al., 2015). To illustrate the effect, we modify the simple fault model of **Figure 1** to include bends and steps in the fault trace (**Figure 3a)**. Each rupture complexity is considered to represent a "challenge" for propagation. We qualitatively illustrate the reduction in probability arising from each challenge with the dashed lines in **Figure 3b**. Probabilities on the left side are lower than on the right because three subsection connections on the right have no bend or step to reduce the probability of continuing.

To quantify the effects of steps and bends, we draw on the results of Biasi and Wesnousky (2016, 2017). Considering step widths first, Biasi and Wesnousky (2016) measured steps in mapped historic surface ruptures. Where fault were mapped beyond the ends of surface rupture, step widths at the ends of ruptures were also measured. For a given step width, the ratio of the number of ruptures that passed to the number of that size that stopped rupture at an end is defined as the passing ratio (**Figure 4a)**. An approximately linear dependence of this ratio on step width is observed for steps from 1 to 6 km. Ruptures are observed to stop or pass through steps of 3 km with approximately equal frequency. A similar passing ratio relationship was observed for bends in surface ruptures, where the size of the angle in the surface trace is observed (**Figure 4b**). For bends, observations show that bends in a fault trace <15° are passed over twice as often as they stop rupture while bends of 31° are twice as likely to stop rupture as to be passed.

Passing ratios for steps and bends in **Figures 4a and b** are converted to probabilities in **Figures 4c and d**, respectively. P_{ab} and P_{as} are the probabilities that a bend or step, respectively, will arrest rupture. The complimentary probabilities, $P_{pb}=1-P_{ab}$ and $P_{ps}=1-P_{as}$, respectively, are interpreted as the probability that a rupture will pass beyond the bend or step. For steps smaller than 1 km, a linear extrapolation is applied in **Figure 4c**. It is assumed that no probability decrease should be applied to rupture continuance when no step is present between panels. The discontinuity in slope at a width of 1 km is considered to be an artifact of insufficient data (Biasi and Wesnousky, 2016) that might be resolved with further study. For the probability of stopping at bends shown in **Figure 4d**, a smoother extrapolation has been used because the range of estimates in passing ratio for angles smaller than 10 degrees is less well defined. We consider a bend of 0 (no bend) to associate with a penalty of 0.

The probability curves of **Figures 4c and 4d** provide the means to quantify consequences of bends and steps of a discrete fault model such as is shown in **Figure 3**. The probability of a rupture lengthened by one subsection is smaller by the "penalty" from the step or bend, applied as a product. The cumulative effect of these penalties for bends and steps means that long, complex ruptures should be rare compared to their incidence on geometrically simpler faults.

Expanding to consider UCERF3 model

The model in **Figure 4** can be extended to the active fault system of California using the fault model in UCERF3 (**Figure 5**). The discrete fault elements are called "subsections". They extend in depth to the base of the local seismogenic zone, and half that (i.e. 5-7 km) in strike length. Fault subsections in UCERF3 can have multiple sub-planes, but to be consistent in scale size with the measurements in Biasi and Wesnousky (2016, 2017), orientations are represented by an average single dip and dip direction. We estimate the dip direction using the strike defined by end points of the subsection. In UCERF3, ruptures consist of a sequence of two or more subsections. Ruptures are limited to single paths with no discontinuities greater than the maximum step size, and no bi-furcations ("Y"-shaped ruptures). The complete set of ruptures receiving rate estimates was defined using rules for geometric compatibility in Milner et al. (2013). The rupture rates themselves were estimated using a Monte-Carlo-based inversion (Field et al., 2014). Rupture geometric complexity was not applied as an a priori probability constraint in the UCERF3 inversion.

The UCERF3 fault model contains the necessary framework to estimate probabilities of eventual length for any rupture on the fault system detected earthquake early warning. If the initial alert is identified with any subsection in the UCERF3 fault model, the effects of bends and steps on rupture extension can be calculated using the probabilities in **Figures 4c and d**. Step distances between subsections are calculated from the separation of fault panels based on the latitudes and longitudes of the ends of the subsections. The angle between fault subsections is computed in 3-D using the average dip and computed dip direction parameters of the subsections. The conditional probability $P_k(L)$ of rupture length L under step and bend effects given initiation at subsection k, is

Eqn 1. $$P_k(L) = \prod P_{sb\_i}$$

where the P_{sb_i} is the step or bend probability connecting adjacent subsections in the rupture and product is over pairs of subsections that comprise length L. Equation 1 applies to unilateral rupture from the initial subsection. For any specific bi-lateral rupture, Eqn 1 is applied once in each direction to cover the full rupture extent, and the probabilities associated with the two directions are multiplied. With application of **Equation 1** to successively longer ruptures, the accumulation of step and bend penalties produces a monotonically declining probability of rupture length.

We illustrate the application of step and bend passing probabilities to estimate rupture length probabilities with two examples from southern California (**Figures 6** and **7**). The first example assumes the earthquake starts at the southeastern end of the San Andreas fault at Bombay Beach (star), and rupture extends unilaterally northwest (**Figure 6**). In **Figure 6,** subsection intersections for the SAF and SJF are shown as dots. From the alert location, the individual bend and step penalties for rupture are computed separately using the geometries of each subsection intersection. The individual bend and step passing probabilities are shown in **Figure 7a** (circles and + symbols, respectively), and the solid line shows their joint application. Cumulative applications of each using **Eqn 1** are shown in **Figure 7b**. We take probabilities of length in our interpretations from cumulative joint probability curve. The SAF northwest from Bombay Beach is relatively straight and smooth. The first significant bend and step complexities are encountered 13 subsections NW at the intersection with the Mill Creek SAF fault section. Other SAF section transitions are indicated in Figure 6. The decline in propagation probabilities north of the Coachella section is consistent with the progressive CCW rotation of fault strike on the Mill Creek to a less favorable orientation for through rupture. Only 5% of ruptures starting on the Coachella section are predicted to get past the Mill Creek section to reach eastern San Bernardino, only 2.5% continue to the near SE end of the Mojave South section (**Figure 7b)**, and only 0.2% would rupture "wall-to-wall" from Bombay Beach to Parkfield. Based on fault geometry, ruptures that start in the southeast end of the San Andreas fault should rarely reach to the eastern edge of metropolitan Los Angeles at San Bernardino.

In the second example, the rupture starts on the San Jacinto fault at the Casa Loma step over (**Figure 6; Figure 8**). In this case, rupture might extend northwest or southeast. Because probabilities in Equation 1 are conditioned on the alert location, probabilities of the NW and SE extents are independent, and thus can be considered separately. In the UCERF3 fault model, the SJF can connect NW to the San Bernardino North SAF two ways, over 3 subsections of the Lytle Creek fault (**Figure 8a, b)** or continue 3 subsections further on the SJF (**Figure 8c**). Based on fault geometry, the direct connection is a more likely path for through ruptures, though neither is very likely to actually continue on the Mojave South section (5.8% vs. 2.7%). Lozos et al. (2015) and Lozos (2016) have studied rupture propagation through this intersection and found that it is sensitive to poorly resolved details of the fault system geometry. For rupture extending to the SE on the SJF, decrements in probability correspond to recognized section boundaries (**Figure 8d)**. Anza and Coyote Creek sections are relatively straight, with little geometric basis for rupture arrest, while curvature of the Borrego fault (**Figure 6**) causes a progressive decrease in probability of through rupture. The probability of any given bilateral rupture extent given a starting alert near the Casa Loma stepover would be the product of probability of the corresponding NW and SE extents.

In Figures 7 and **8** we so far have discussed conditional probabilities of length on a single rupture paths. This may be sufficient for some purposes. However, if conditional probability of length or

magnitude is required regardless of path, an accounting must be made of probabilities at branch points. As long as the paths are independent alternatives, probabilities of a given rupture length or magnitude can be combined by weighting by their relative geometric probabilities at the branch point. Using the example in **Figure 8** of connection from the SJF to the SAF directly versus by Lytle Creek, the last common point is on the San Jacinto San Bernardino strand (SJSB, **Figures 8b and c**). Staying on the SJF involves a bend probability of 0.76, and no step penalty. Jumping to the Lytle Creek fault involves a slightly larger bend penalty of 0.64 and a small step with penalty, 0.91. Combining, gives probabilities of 0.76 vs. 0.58, respectively. Thus, based on fault geometric parameters, the direct connection is preferred. Probabilities of length on the direct connection path would be weighted by 0.76/(0.76+0.58) = 57% vs. 43% for connection by Lytle Creek. Weighting of this sort applies to length or magnitude accumulated on distinct branches. In this case, the alternate paths meet on the Mojave South section. NW of that intersection, the probabilities of length in **Figures 8b and 8c** can be summed. Alternative weighting approaches are discussed in a later section.

UCERF3 Rupture Length Predictions

If rupture probabilities are available for all possible ruptures and paths, these probabilities can provide a third basis for the conditional probability of rupture length given EEW initiation. Such probabilities are available for California from UCERF3 (Field et al., 2014). From the complete set of ruptures and probabilities, it is possible to extract subsets for a desired path and starting subsection. We illustrate this process for the San Jacinto fault starting point considered previously. We extract all ruptures in the UCERF3 Fault Model 3.1 NW and having one end at the Casa Loma step, and plot their annual rates of occurrence (star symbols, **Figure 9a**). There are 769 ruptures with this geometry. The solid line above these points summarizes rupture rates in bins of 0.1 **M** units. This line represents the incremental magnitude-frequency curve of all ruptures with one end at the Casa Loma step over. When the logarithmic rate axis is considered, it is seen that the greatest weight (probability of occurrence) is on ruptures of **M** 7.5 or greater.

The assumption that the earthquake has started provides a basis to project UCERF3 annual probabilities into a conditional probability of length function. The UCERF3 rupture set was constructed to give rates for all possible ruptures in the discretized fault model, so the subset with an end at the Casa Loma step over defines a total probability for ruptures with that geometry. Before rupture starts, the probability of any rupture in the set is small, but once we say the Casa Loma step subsection is at one end, with probability 1, the final rupture will be one from the set.

The annual rates of occurrence shown for ruptures shown in **Figure 9a** assume that rupture could nucleate anywhere on their length. For the EEW case, the nucleation point is a specific case. To adjust rates for our constrained nucleation point, we assume the earthquake might nucleate with equal likelihood in any given subsection of a rupture. We thus reduce the annual probability of occurrence for each rupture in **Figure 9a** by $1/n$ where n is the number of subsections in the rupture. The dashed line of **Figure 9b** incorporates this reduction and so represents the UCERF3-based probability of rupture length for unilateral rupture northwest from the Casa Loma step over. The result is shown in terms of probability of earthquake magnitude in **Figure 9c**. In terms of expectations for length, 18% that start at the Casa Loma step over are expected to reach 70 km in length and **M** 7.1. About 16% will continue over 200 km, as **M** 7.6 or larger events. This compares with a probability of 5.4% (summing **Figures 8b** and **8c** at 30 subsections) based on geometry alone.

The UCERF3 rupture model also supports tracking of probability of length or magnitude through bifurcations in the fault. In **Figure 9,** we considered probability of length without specifying exactly which fault(s) the rupture might occupy. Thus, in the set shown, some ruptures join the SAF from the SJF both directly to the SAF north San Bernardino section, and alternately on the Lytle Creek section. Where it is desirable to track such distinctions, the process with **Figure 9** is repeated, but with the rupture set separated by fault branch. Probabilities for each branch at the "Y" are estimated according to the total UCERF3 probability of ruptures that continue. Similarly, bilateral length probabilities conditioned on the initiation point are formed by gathering the SE and NW sets separately in the example of **Figure 8**, then

multiplying the probabilities of length on either side. The eventual magnitude probabilities, however, must be scaled from the combined lengths using a relationship such as in Anderson et al. (2017).

Discussion

Fault-geometric passing probabilities provide an empirical basis for estimating potential rupture lengths given an initiation point on the fault system. Probabilities reflect a "time-independent" estimate, using averages over many historical ruptures, in the same sense as the passing probabilities used to create them. And although we have motivated the research by its application to EEW, conditional length estimates are equally applicable in other contexts where probabilities of rupture extent are needed for hazard scenarios and response planning.

We find for representative nucleation points on southern California's most active faults that realistic probabilities of rupture length can be formed directly from probabilities at geometric complexities. The relatively low probabilities that we find for a rupture extending from the southernmost San Andreas fault into San Bernardino or beyond (Figure 7) are consistent with geologic and dynamic modeling assessments that such a rupture should be rare. For rupture NW from the northern San Jacinto fault (**Figure 8**) we find lower probabilities than from UCERF3 by about a factor of 2 that rupture should extend onto the San Andreas fault. For long, straight faults, some adjustment of rupture probabilities beyond fault-geometric passing probabilities might be considered if shorter ruptures are known to be more likely than long ones. Reasonable adjustments can be achieved with a Gutenberg-Richter or similar fault system magnitude-frequency distribution. Alternatively, the straight portions of faults with no notable geometric complexity may give a physical basis for some measure of characteristic earthquake behavior.

For long ruptures, probability estimates of rupture length or eventual rupture magnitude will require either picking a single fault rupture path, or a means to include probabilities across fault branching. We illustrated an approach using relative weights based on geometric favorability at the intersection providing alternate paths NW from the San Jacinto fault (**Figure 8**). If there were further branches, this procedure could be applied recursively. One might alternatively weight branch probabilities on the basis of relative slip rates of the branches. Using the UCERF3 fault model, slip rates on the SJF and Lytle Creek where they split are 9.0 mm/yr and 1.8 mm/yr, respectively. On this basis, a weighting is found of 83% vs. 17%, respectively, compared to 57% vs. 43% found from geometry alone. A related division might be calculated by summing rupture rates on each branch from the UCERF3 time-independent model.

For specific branch points, paleoseismic data might also provide a basis to adjust respective weightings of branches. Schwartz et al. (2012) show that the eastern extent of the Denali fault had a more recent large surface rupture earthquake on it than the Totchunda fault near their intersection. When the Denali earthquake rupture propagated east, it took the less geometrically favored branch, they infer, because of the more recent previous Denali event. While potentially useful at individual branches, the application of paleoseismic data in this way would be situation-specific. For California, a generalization of this type of data is available through the time-dependent version of UCERF3 (Field et al., 2015). Its use in estimating conditional probabilities of rupture length reserved for future research.

Beside probability of length or magnitude, other questions might be asked, such as the probabilities of magnitude for ruptures that could reach a certain point, such as an urban area. For a conditional probability question such as this, one must consider all combinations of SE and NW extent affecting the city. This would require a certain level of bookkeeping, as illustrated with **Figure 1**, but not comprise an entirely new approach.

For EEW applications, probabilities of length and/or magnitude from any initiation point in the fault model could readily be precompiled. If precompiled, then during an EEW alert, length probabilities can be accessed very quickly by means of look-up table. Such a lookup will not take the place of dynamic estimates of magnitude such as are provided by the FinDer algorithm (Bose et al., 2012, 2015), but length probabilities may be useful for alert area updates.

We motivated this research by considering probabilities of rupture length from an EEW initial alert. During an EEW rupture, precision in the estimate will be secondary to the need to quickly extend the alert

area for a growing rupture. If the question is instead, how do we set policy for an alert area given a growing rupture, the methods developed here could inform the discussion. For example, if an alert earthquake reaches M6, say, on the SE San Andreas fault, are the growth probabilities high enough that all of Los Angeles should be alerted? What about an alert on the southern San Jacinto fault? Are the differences in probability large enough to have fault-specific policies? The methods outlined here can provide input to those decisions.

Beyond application to rupture length estimates, fault-geometric passing probabilities provide complimentary model evaluation metrics for a future UCERF model. UCERF3 ruptures start with no a priori probability per se. If a rupture passes basic geometric compatibility tests (Milner et al., 2013), nothing downstream in the rupture rate inversion distinguishes simple vs. geometrically complex ruptures. Mathematical relationships implementing fault geometric passing probabilities might be formulated, for example, to constrain the ratio of through ruptures to ruptures that stop at a geometric feature. Alternatively, fault-geometric probabilities could be used as a complimentary tool to identify ruptures that pass the Milner et al. (2013) screening, but include multiple, unfavorable geometric intersections and thus could be culled from the rupture set. Shaw et al. (2018) show as long as fault slip rates are matched in the rupture set, hazards and ground motion estimates will match the full rupture set. A smaller input rupture set would improve computational performance of the rate inversion. Finally, instead of using fault geometric probabilities as inputs to the inversion, they could be used to compare with inversion results. The UCERF3 model has been difficult for geologists to evaluate (e.g., Schwartz, 2018) because virtually all available geologic data are used as inputs to the inversion. Once the data are fit by the inversion, little independent data remain to evaluate the resulting model. Geometrically based passing probabilities cannot directly replace a rupture rate inversion, but they do make specific, physically grounded predictions of the relative rates of long and short ruptures and these data are not inputs to the UCERF3 inversion. Summarizing, step and bend complexities model geometry well, without reference to slip rate, and UCERF3 fits slip rate without reference to geometric complexity.

Conclusion

A fault-geometric approach is presented to estimate the conditional probabilities of rupture length and/or magnitude, based on probabilities of passing bend and step structures. Fault geometric complexities, when translated to probabilities of rupture arrest, comprise challenges a rupture encounters serially in order to increase in length. The probability of length is thus the product of the complimentary probabilities of continuing. Long and complex ruptures are, as a consequence, less frequent, conforming to empirical observation. For example nucleation points on the San Andreas and San Jacinto faults in southern California, the derived probability of length estimates conform to expectations that ruptures are likely to be arrested in by the significant change in fault strike of the Mill Creek and eastern north San Bernardino sections. Only 2% of ruptures starting at Bombay Beach are predicted to extend onto the southern Mojave section of the fault. Based on fault geometric complexity, fewer than 10% that initiate on the NW San Jacinto fault would proceed onto the southern San Andreas fault.

One may also extract conditional length probabilities directly from the UCERF3 rupture rates. This use of UCERF3 assumes that the conditional probability of rupture length given a nucleation point can be interpreted from the time-independent rupture rate forecast. In a point comparison for the northern San Jacinto fault, conditional probabilities of length systematically favor longer ruptures than from geometric complexity. Fault-geometric probabilities could also play a role in future UCERF models, either as a data constraint, a compliment to model construction, or as a tool to evaluate inversion results. Fault-geometric features exert physically significant effects on ruptures, so their inclusion in future UCERF models would be a step toward a more physically based rupture rate model.

In an earthquake early warning context, the methods developed here provide a basis to estimate where a rupture may go, and with what probabilities. These probabilities are readily compiled in advance for any given starting subsection in the fault model, in effect covering likely nucleation locations for large earthquakes anywhere in the California fault network. These probabilities could be used before the event to advise policy about alerting extent for different faults. Operationally, pre-compiled probabilities could

quickly be accessed by the EEW system when an earthquake has initiated. As an immediately useful result, we find that an earthquake that initiates at Bombay Beach on the SE end of the San Andreas fault only reaches San Bernardino about 5% of the time, the point at which modeling suggests a major risk to Los Angeles.

Data Sources

All data used in this paper are from published sources in cited references.

Acknowledgements

This research was supported by the Southern California Earthquake Center Awards 17064 and 12012 (Contribution No. XXXX). SCEC is funded by NSF Cooperative Agreement EAR-1600087 & USGS Cooperative Agreement G17AC00047. Center for Neotectonics Studies Contribution #XX.

References

Allen, R. M. and H. Kanamori, 2003. The potential for earthquake early warning in Southern California, *Science 300*, 786-789.

Allen, R. M., P. Gasparini, O. Kamigaichi and M. Böse, 2009. The status of earthquake early warning around the world: An introductory overview, *Seismol. Res. Lett., 80*, 682-693.

Anderson, J. G., G. P. Biasi and S. G. Wesnousky, 2017. Fault-scaling relationships depend on the average fault-slip rate. *Bull. Seismol. Soc. Am., 107,* 2561-2577.

Biasi, G. P. and S. G. Wesnousky, 2016. Steps and gaps in ground ruptures: empirical bounds on rupture propagation, *Bull. Seismol. Soc. Am., 106,* 1110-1124.

Biasi, G. P. and S. G. Wesnousky, 2017. Bends and ends of surface ruptures, *Bull. Seismol. Soc. Am., 107,* 2543-2560.

Böse, M., C. Felizardo, and T. H. Heaton (2015). Finite-fault rupture detector (FinDer): Going real-time in Californian ShakeAlert system, *Seismol. Res. Lett. 86*, 1692-1704.

Böse, M., T. H. Heaton, and E. Hauksson (2012). Real-time finite fault rupture detector (FinDer) for large earthquakes, *Geophys. J. Int., 191*, 803–812.

Chung, A. I., I. Henson, and R. M. Allen (2019). Optimizing earthquake early warning performance: ElarmS-3, *Seismol. Res. Lett., 90*, 727-743.

Cochran, E. S., J. Bunn, S. E. Minson, A. S. Baltay, D. L. Kilb, Y. Kodera, and M. Hoshiba (2019). Event detection performance of the PLUM earthquake early warning algorithm in southern California, *Bull. Seismol. Soc. Am., 109*, 1524-1541.

Cooper, J.D., 1868. Cooper J. D. San Francisco Daily Evening Bulletin November 3.

Field, E. H., T. H. Jordan, M. T. Page, K. R. Milner, B. E. Shaw, T. E. Dawson, G. P. Biasi, T. Parsons, J. L. Hardebeck, A. J. Michael, R. J. Weldon, P. M. Powers, K. M. Johnson, Y. H. Zeng, K. R. Felzer, N. van der Elst, C. Madden, R. Arrowsmith, M. J. Werner, and W. R. Thatcher, 2017. A synoptic view of the Third Uniform California Earthquake Rupture Forecast (UCERF3). *Seismol. Res. Lett., 88*, 1259-1267.

Field, E. H., G. P. Biasi, P. Bird, T. E. Dawson, K. R. Felzer, D. D. Jackson, K. M. Johnson, T. H. Jordan, C. Madden, A. J. Michael, K. R. Milner, M. T. Page, T. Parsons, P. M. Powers, B. E. Shaw, W. R. Thatcher, R. J. Weldon, and Y. Zeng (2015). Long-term, time-dependent probabilities for the Third Uniform California Earthquake Rupture Forecast (UCERF3), *Bull. Seism. Soc. Am. 105*, 511–543.

Field, E. H., R. J. Arrowsmith, G. P. Biasi, P. Bird, T. E. Dawson, K. R. Felzer, D. D. Jackson, K. M. Johnson, T. H. Jordan, C. Madden, A. J. Michael, K. R. Milner, M. T. Page, T.

406 Parsons, P. M. Powers, B. E. Shaw, W. R. Thatcher, R. J. Weldon, R.J., and Y. H. Zeng,
407 2014. Uniform California Earthquake Rupture Forecast, Version 3 (UCERF3) -The time-
408 independent model. *Bull. Seismol. Soc. Am., 104*, 1122-1180.
409 Harris, R. A., R. J. Archuleta and S. M. Day, S.M., 1991. Fault steps and the dynamic rupture
410 process - 2-D numerical simulations of a spontaneously propagating shear fracture. *Geophy.*
411 *Res. Lett. 18*, 893-896.
412 Heaton, T. H., 1985. A model for a seismic computerized alert network. *Science 228*, 987-990.
413 Kanamori, H., E. Hauksson, and T. Heaton, 1997. Real-time seismology and earthquake hazard
414 mitigation, *Nature 390*, 461-464.
415 Kanamori, H., P. Maechling, and. E. Hauksson, 1999. Continuous monitoring of ground-motion
416 parameters. *Bull. Seismol. Soc. Am., 89*, 311-316.
417 Kanamori, H., 2005. Real-time seismology and earthquake damage mitigation, *Ann. Rev. Earth*
418 *and Planet. Sci. Lett., 33*, 195-214.
419 Kodera, Y. (2018). Real-time detection of rupture development: Earthquake early warning using
420 P waves from growing ruptures, *Geophys. Res. Lett. 45*, 156–165.
421 Kohler, M. D., E. S. Cochran, D. Given, S. Guiwits, D. Neuhauser, I. Henson, R. Hartog, P.
422 Bodin, V. Kress, S. Thompson, C. Felizardo, J. Brody, R. Bhadha, and S. Schwarz (2018).
423 Earthquake early warning ShakeAlert system: West Coast wide production prototype,
424 *Seismol. Res. Lett., 89*, 99-107.
425 Lettis, W., J. Bachhuber, R. Witter, C. Brankman, C. E. Randolph, A. Barka, W. D. Page, and A.
426 Kaya (2002). Influence of releasing step-overs on surface fault rupture and fault
427 segmentation: Examples from the 17 August 1999 Izmit earthquake on the North Anatolian
428 fault, Turkey, *Bull. Seismol. Soc. Am., 92*, 19-42.
429 Lozos, J. C. (2016). A case for historic joint rupture of the San Andreas and San Jacinto faults,
430 *Science Advances, 2:e1500621*, 7 p.
431 Lozos, J.C., D. D. Oglesby, B. Duan, and S. G. Wesnousky (2011). The effects of double fault
432 bends on rupture propagation: A geometrical parameter study, *Bull. Seismol. Soc. Am., 101*,
433 385-398.
434 Lozos, J. C., D. D. Oglesby, J. N., Brune, and K. B. Olsen (2015). Rupture propagation and
435 ground motion of strike-slip stepovers with intermediate fault segments, *Bull. Seism. Soc.*
436 *Am., 105*, 387-399.
437 Meier, M.-A., T. Heaton, and J. Clinton (2016). Evidence for universal earthquake rupture
438 initiation behavior, *Geophys. Res. Lett., 43*, 7991-7996.
439 Milner, K., M. T. Page, E. H. Field, T. Parsons, G. Biasi, and B. E. Shaw (2013). Defining the
440 inversion rupture set via plausibility filters, U.S.G.S Open-File Report 2013-1165, Uniform
441 California Earthquake Rupture Forecast Version 3 (UCERF3) – The Time-Independent
442 Model, Appendix T, 14 pp.
443 Nakamura, Y., 1988. On the urgent earthquake detection and alarm system (UrEDAS).
444 *Proceedings of the Japanese National Committee of the Inernational Association for*
445 *Earthquake Engineering VII*, 224-238.
446 Noda, S. and W. L. Ellsworth (2016). Scaling relation between earthquake magnitude and the
447 departure time from P wave similar growth, *Geophys. Res. Lett., 43*, 9053-9060.
448 Olson, E. L. and R. M. Allen (2005). The deterministic nature of earthquake rupture, *Nature,*
449 *438*, 212-215.
450 Schwartz, D. P. (2018). Past and future fault rupture lengths in seismic source characterization –
451 The long and short of it, *Bull. Seismol. Soc. Am., 108,* 2493-2520.

Schwartz, D. P., P. J. Haeussler, G. G. Seitz, and T. E. Dawson (2012). Why the 2002 Denali fault rupture propagated onto the Totschunda fault: Implications for fault branching and seismic hazards, *J. Geophys. Res., 117*, B11304.

Shaw, B. E., K. R. Milner, E. H. Field, K. Richards-Dinger, J. J. Gilchrist, J. H. Dieterich, and T. H. Jordan (2018). A physics-based earthquake simulator replicates seismic hazard statistics across California, *Science Advances, 4*, eaau0688, 9 pp.

Trugman, D. T., M. T. Page, S. E. Minson, and E. S. Cochran (2019), Peak ground displacement saturates exactly when expected: Implications for earthquake early warning, *J. Geophys. Res. Solid Earth, 124*, 4642-4653.

Wu, Y.M. and T. L. Teng, 2002. A virtual subnetwork approach to earthquake early warning. *Bull. Seismol. Soc. Am., 92*, 2008-2018.

Wu, Y. M. and H. Kanamori, 2005. Rapid assessment of damge potential of earthquakes in Taiwan from the beginning of P waves. *Bull. Seismol. Soc. Am., 95*, 1181-1185.

Wu, Y. M., H. Kanamori, R. M. Allen and E. Hauksson, 2007. Determination of earthquake early warning parameters, tau(c) and P-d, for southern California. *Geophys. J. Int., 170*, 711-717.

Wu, Y. M. and H. Kanamori, 2008. Development of an earthquake early warning system using real-time strong motion signals. *Sensors, 8*, 1-9.

Yamada, T. and S. Ide (2008). Limitation of the predominant-period estimator for earthquake early warning and the initial rupture of earthquakes, *Bull. Seismol. Soc. Am., 98*, 2739-2745.

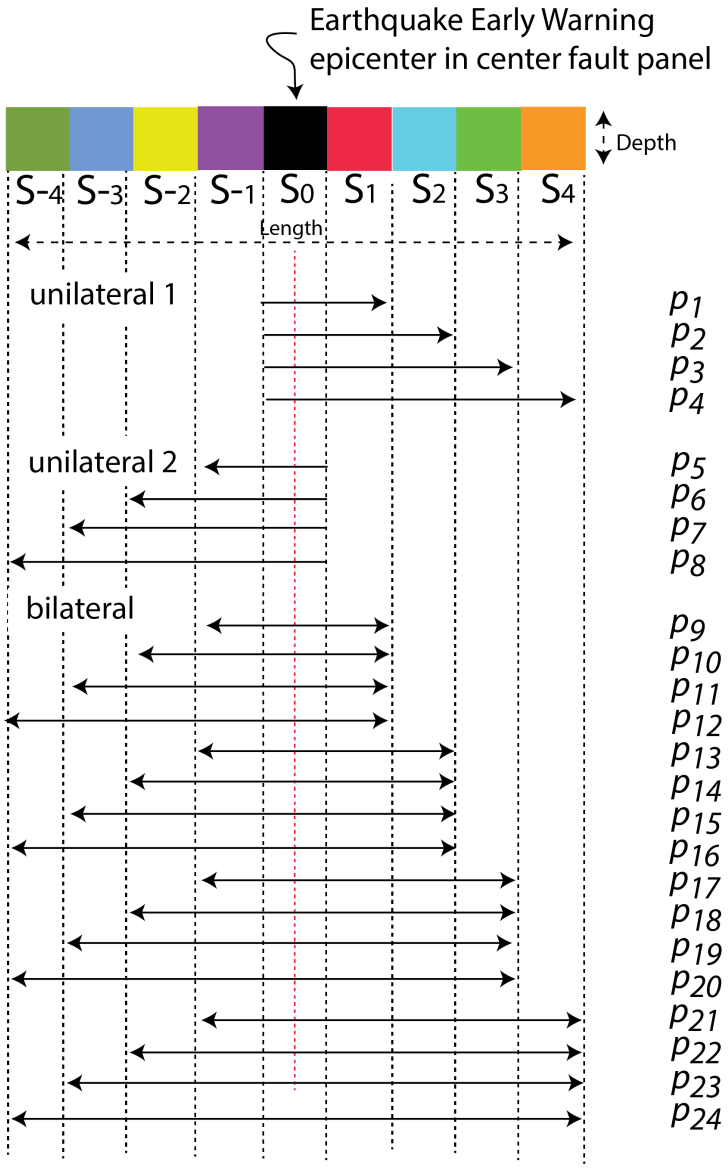

Figure 1. Illustration of single fault composed of 9 panels (subsections) illustrating possible rupture extents for an earthquake initiating in central panel S_0. The probability of any given rupture is p_i.

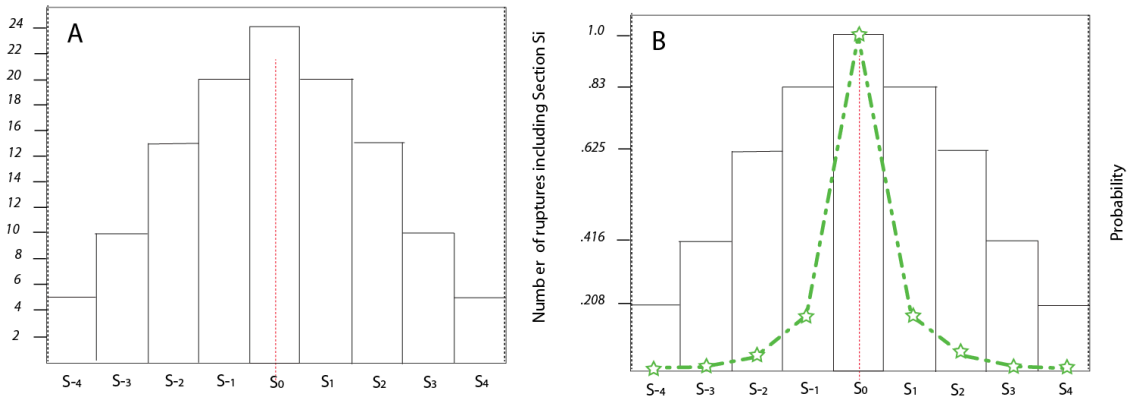

Figure 2. (A) Histogram showing the number of ruptures each subsection could participate in. (B) Probability of a subsection being involved in rupture given rupture initiates in S_0 and each possible rupture is considered equally likely. Dashed line and stars illustrate reduction in probabilities if a power-law distribution exists among likely rupture lengths on the model fault. See text for further discussion.

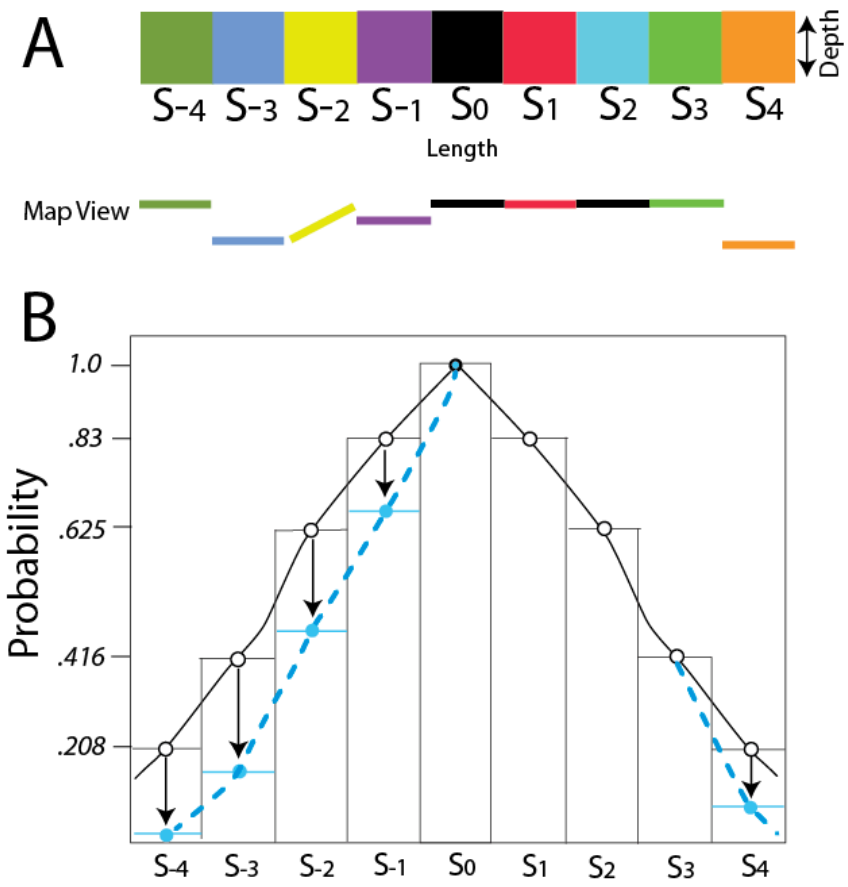

Figure 3. (A) Fault model with panel boundaries containing steps and bends in fault trace. (B) The probabilities of a rupture extending from panel S_0 to others in the fault model. Open circles and solid line result if all ruptures are considered equally likely; the dashed line with filled circles reflect qualitatively the reduction in probability of length when penalties for passing are applied at panel boundary steps or bends.

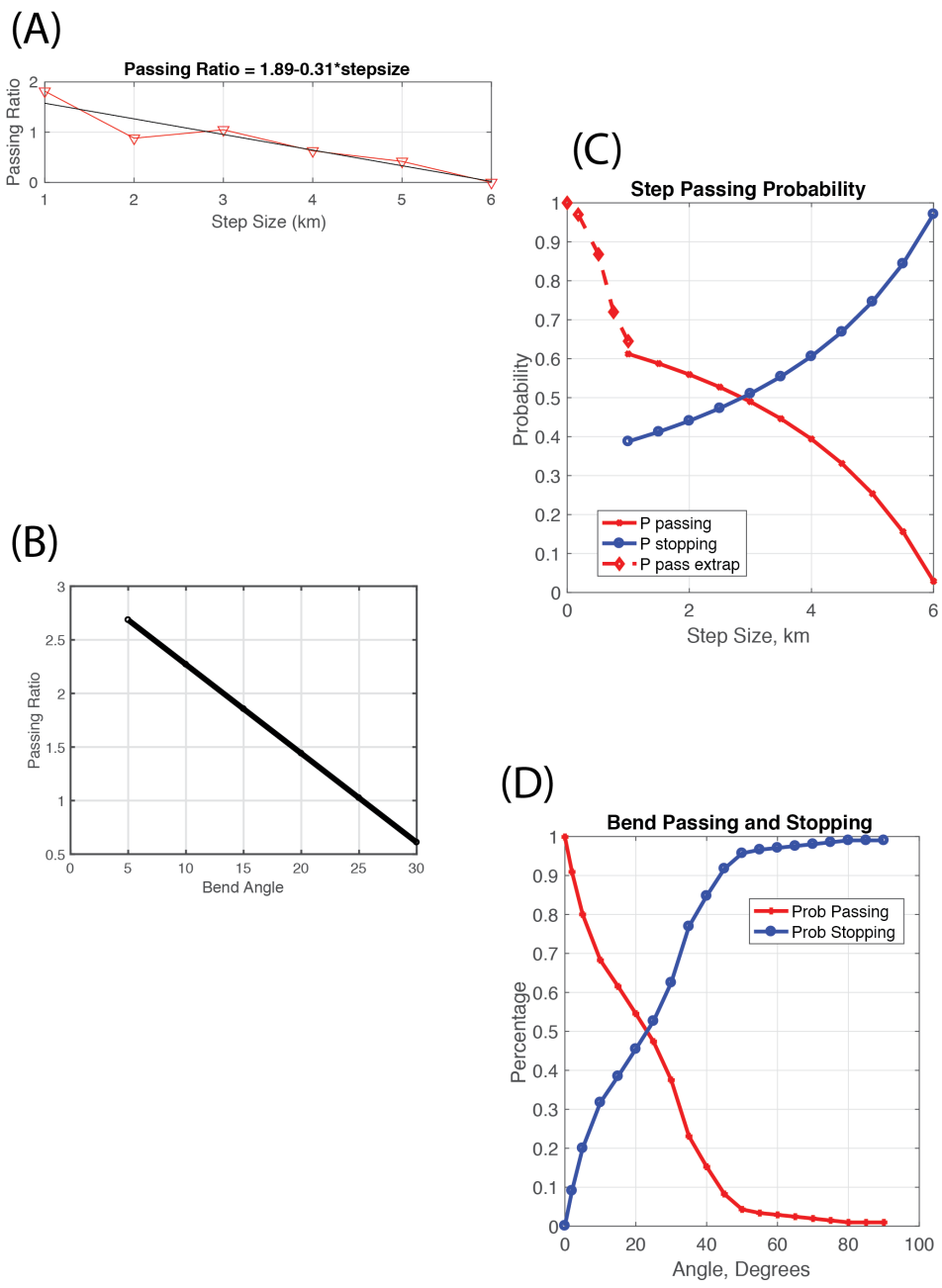

Figure 4. Passing ratios versus (A) step width and (B) bend angle, adapted from Biasi and Wesnousky 2016 and 2017, respectively. Bend and step complexities are measured between fault sections of at least 5-7 km in length. (C) Probability of passing or stopping at a step vs. step width (P_{ps} and P_{as}, respectively in the text). (D) Probability of passing or stopping at a bend of given angle in fault trace (P_{pb} and P_{ab}, respectively).

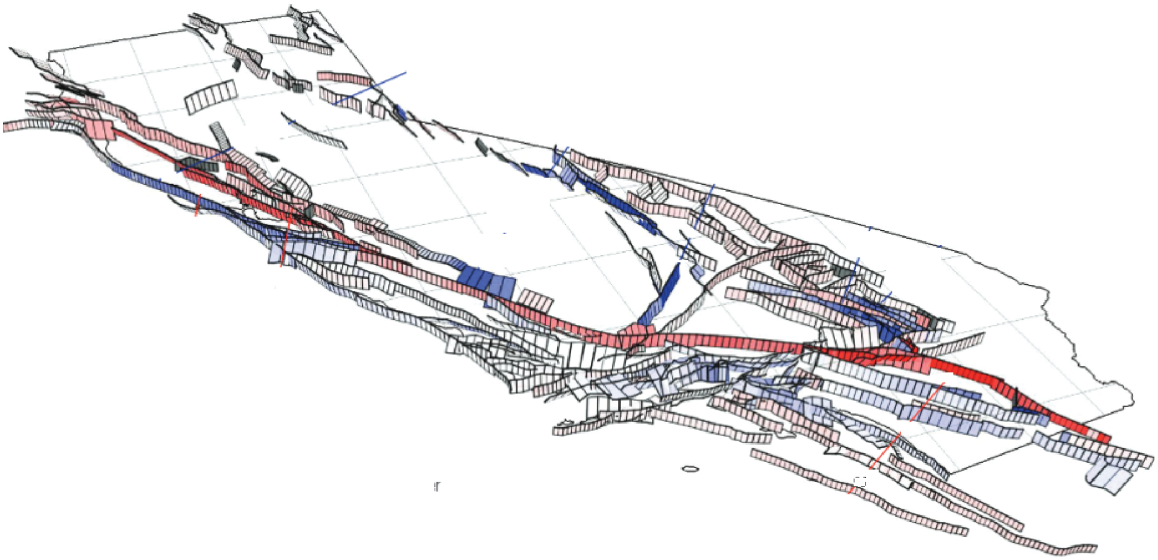

Figure 5. Discrete fault model FM3.1 from UCERF3. Faults are shaded by slip rate. Figure from Field et al. (2014).

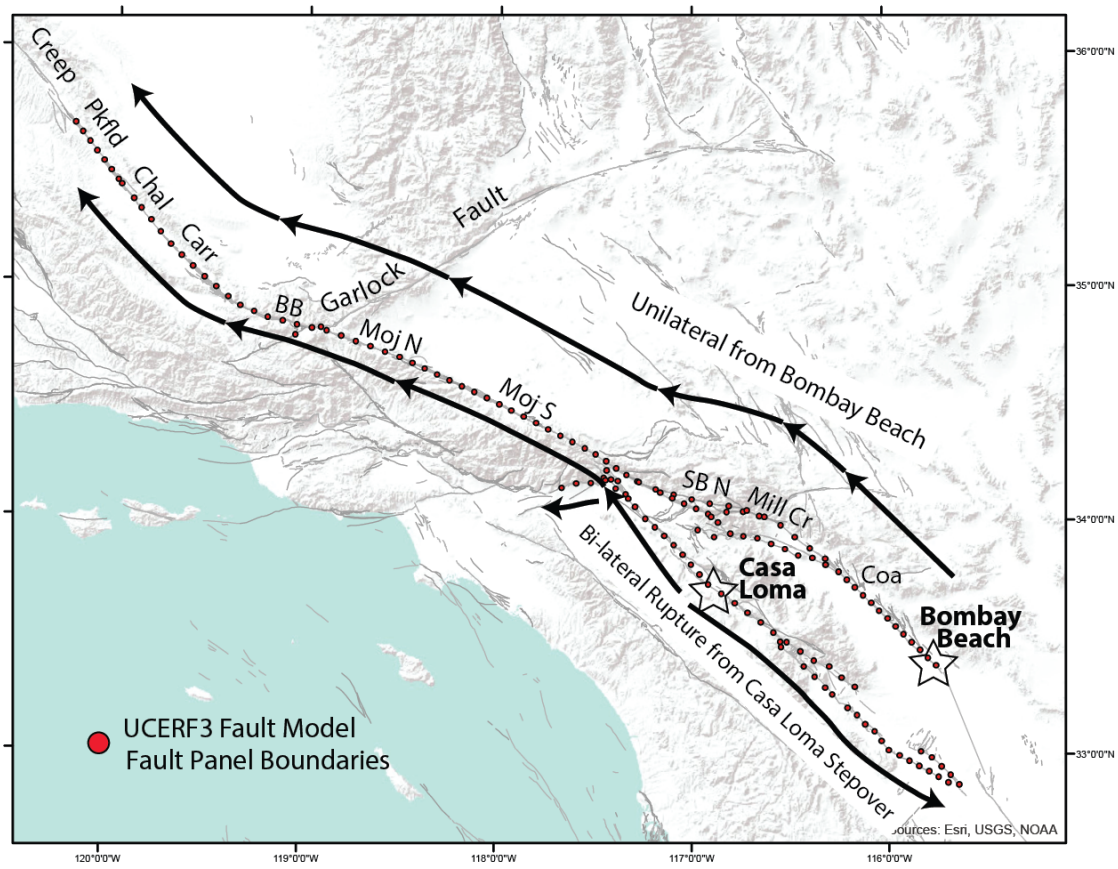

Figure 6. Example paths of rupture propagation given earthquake initiation points (stars) on two major southern California faults. Rupture starting at Bombay Beach (eastern star) is modeled on the San Andreas fault for its full length. Rupture northward on the San Jacinto fault (western star) begins at the Casa Loma stepover then transitions to the San Andreas fault either directly, or by a short section of the Lytle Creek fault. Rupture may also extend south from the Casa Loma starting point.

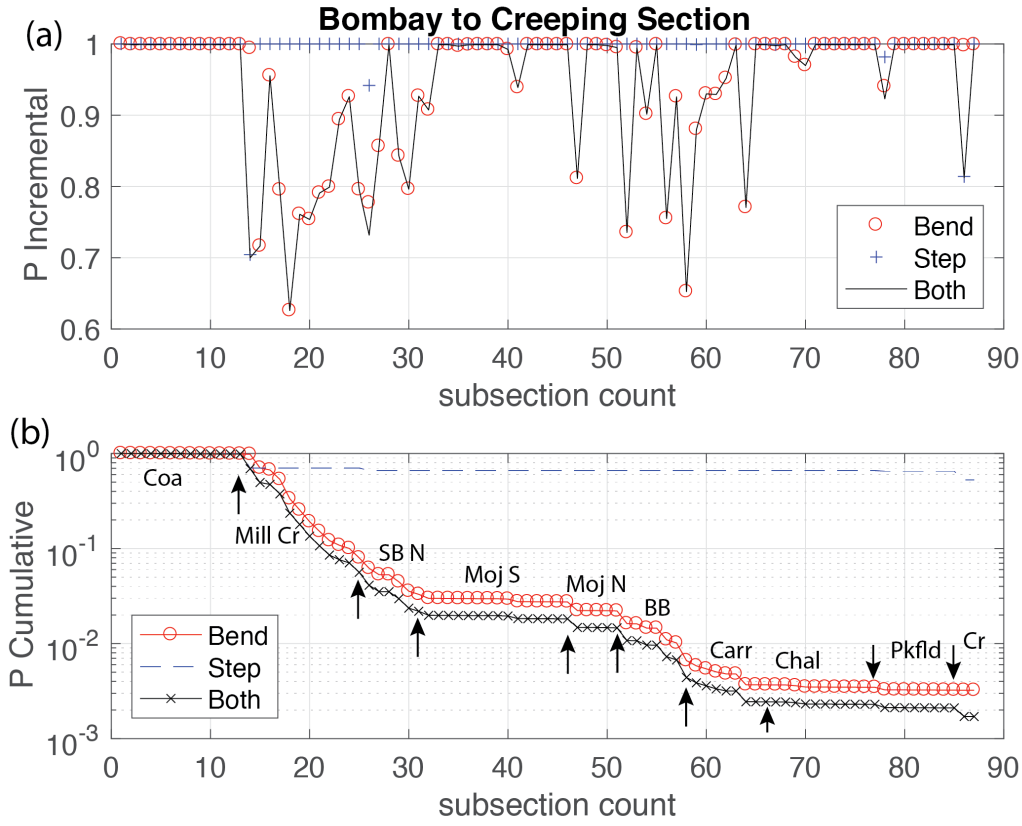

Figure 7. Geometric and cumulative passing probabilities at subsection boundaries for a unilateral rupture NW from Bombay Beach. (A) Individual probabilities of continuing through subsection bend ("o") and step ("+") intersections. Solid line shows their joint application. Subsections are ~7 km in length. Fault portions that are straight with no steps have no geometric basis for arresting rupture. (B) Cumulative application of bend (circles) and step (dashed) penalties given initiation at Bombay Beach. "x" symbols show their joint application. Text labels indicate UCERF3 fault sections. Coa: Coachella; Mill Cr.: Mill Creek; SB N: San Bernardino North; Moj S: Mojave South; Moj N: Mojave North; BB: Big Bend; Carr: Carrizo; Chal: Chalome; Pkfld: Parkfield; Cr: SE end of creeping section. Arrows mark section intersections.

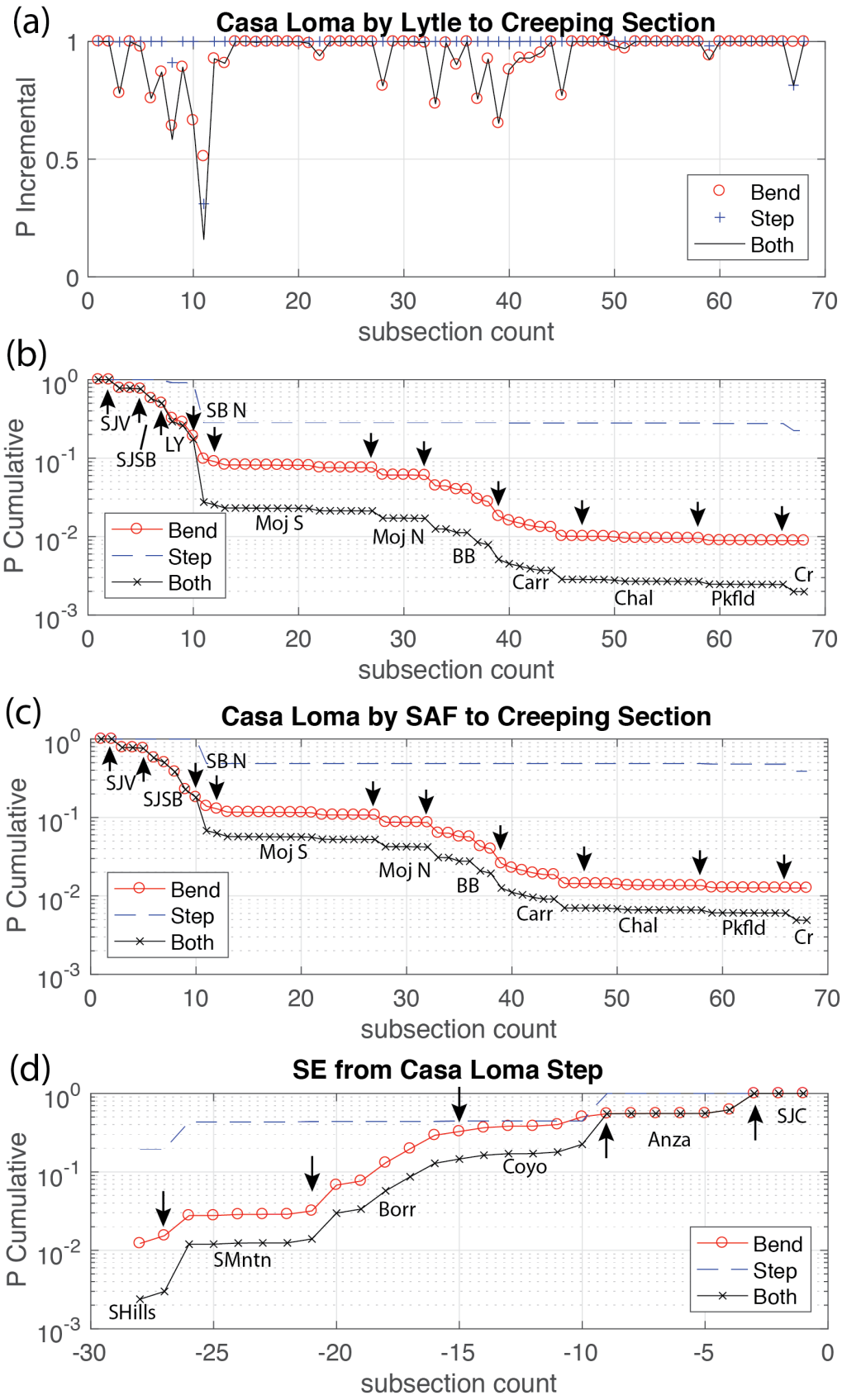
(a)
Casa Loma by Lytle to Creeping Section
P Incremental
subsection count
Bend
Step
Both
(b)
P Cumulative
SJV
SJSB
LY
SB N
Moj S
Moj N
BB
Carr
Chal
Pkfld
Cr
subsection count
(c)
Casa Loma by SAF to Creeping Section
P Cumulative
SJV
SJSB
SB N
Moj S
Moj N
BB
Carr
Chal
Pkfld
Cr
subsection count
(d)
SE from Casa Loma Step
P Cumulative
SHills
SMntn
Borr
Coyo
Anza
SJC
subsection count

556

Figure 8. Geometric and cumulative penalties at subsection boundaries for rupture NW and SE from the San Jacinto Claremont-Casa Loma step over. (a) Individual step ("+" and dashed) and bend passing probabilities ("o") on the paths of rupture extending (a) unilaterally NW onto the San Andreas fault by Lytle Creek to the SAF. (b) Cumulative probability of length for (a). Arrows mark section intersections. (c) Cumulative probability for an alternate path where the San Jacinto fault connects directly to the SAF directly from the San Bernardino strand of the SJF. (d) Conditional probability of rupture length unilaterally southeast from the Casa Loma starting point. The fault-geometric estimate of probability of any length bi-lateral rupture is the product of the two unilateral estimates. Section names - SJV: San Jacinto Valley; SJSB: San Jacinto San Bernardino; LY: Lytle Creek; SJC: San Jacinto Stepover Combined; Anza: San Jacinto Anza; Coyo: SJF Coyote Creek section; Borr: Borrego; SMntn: Superstition Mountain; SHills: Superstition Hills. Other abbreviations given with Figure 7.

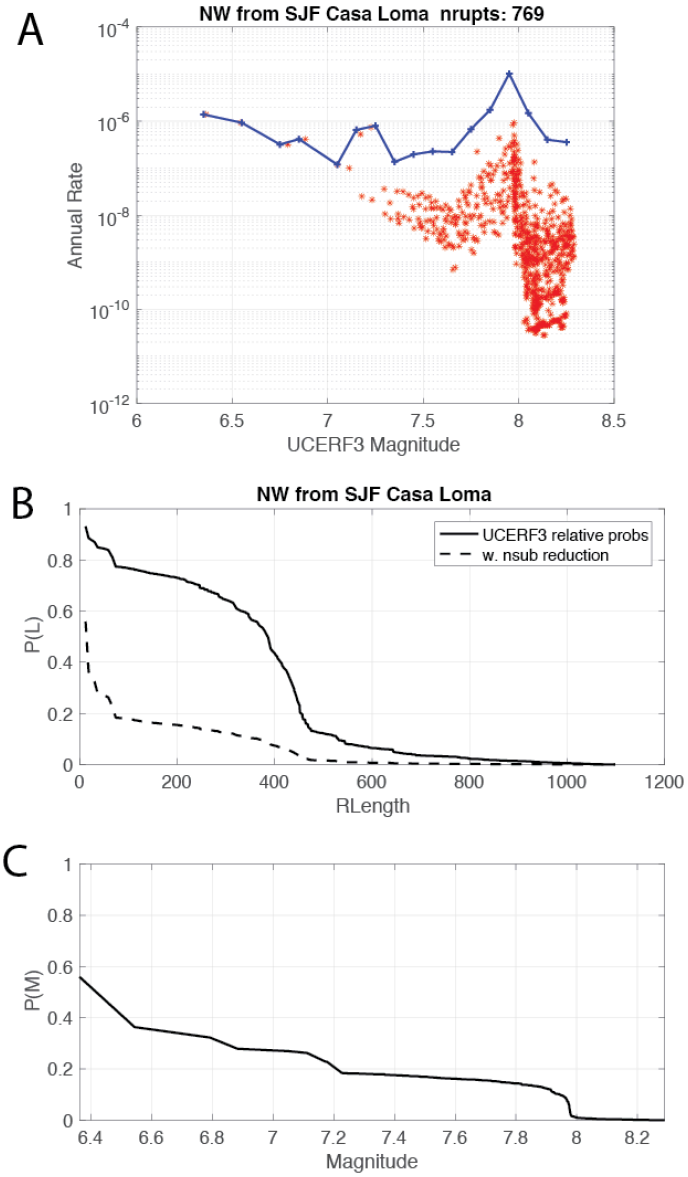

Figure 9. UCERF3-based rupture length probabilities for rupture starting at the San Jacinto Casa Loma step. (A) Individual annual rupture rates (probabilities) (stars) and incremental magnitude-frequency distribution (solid line, binned at 0.1 magnitude units) of all ruptures in UCERF3 Fault Model 3.1 that end at the Casa Loma step of the San Jacinto fault (west star, **Figure 6**). (B) The corresponding complimentary cumulative distribution (CCD) (solid line) of rupture length for ruptures in (A). Dashed line shows the length CCD if individual rupture probabilities are reduced by the number of subsections (=initiation points) in the rupture. (C) CCD for rupture magnitude for the reduced CCD curve in (B). By this estimate, 54% of single subsection EEW initiations grow to **M** 6.3, 25% become **M** 6.9 to 7.1, and 16% become **M** 7.6 or larger.